

# Free-surface flows past a surface-piercing object of finite length

By J. ASAVANANT AND J.-M. VANDEN-BROECK

Department of Mathematics and Center for the Mathematical Sciences,  
University of Wisconsin-Madison, Madison, WI 53705, USA

(Received 12 August 1993 and in revised form 8 February 1994)

Steady two-dimensional flows past a parabolic obstacle lying on the free surface in water of finite depth are considered. The fluid is treated as inviscid and incompressible and the flow is assumed to be irrotational. Gravity is included in the free-surface condition. The problem is solved numerically by using boundary integral equation techniques. It is shown that there are solutions for which the flow is supercritical both upstream and downstream and others for which the flow is subcritical both upstream and downstream. These flows have continuous tangents at both ends of the obstacle at which separation occurs. For supercritical flows, there are up to three solutions corresponding to the same value of the Froude number when the obstacle is concave and up to two solutions when the obstacle is convex. For subcritical flows, there are solutions with waves behind the obstacle. As the Froude number decreases, these waves become steeper and the numerical calculations suggest that they, ultimately, reach limiting configurations with a sharp crest forming a  $120^\circ$  angle.

---

## 1. Introduction

This paper is devoted to the study of two-dimensional steady flows past a curved object lying on a free surface in water of finite depth (see figure 1). Even though this is a two-dimensional problem, it can be used to model some real flows, e.g. a ship or a barge-like vessel moving at a constant velocity in a channel.

Over the last two hundred years, many approximate solutions have been obtained by linearizing the equations around a uniform stream with constant velocity  $U$  and constant depth  $H$ . The properties of these linear solutions are characterized by the Froude number

$$F = \frac{U}{(gH)^{1/2}}, \quad (1)$$

where  $g$  is the acceleration due to gravity. If  $F > 1$ , the flow is called supercritical and is characterized by a uniform stream in the far field (see figure 1*a*). If  $F < 1$ , the flow is called subcritical and is characterized by a train of waves downstream (see figure 1*b*). In this paper, we solve the complete nonlinear equations numerically. Although the value  $F = 1$  is not a significant critical value for nonlinear solutions, we still refer to solutions with  $F < 1$  as subcritical and to solutions with  $F > 1$  as supercritical.

It is not obvious that there are flows with continuous free-surface profiles such as those sketched in figure 1. A possible kind of discontinuity is the breaking of the free surface near the leading contact point B. In water of infinite depth, previous investigators (Vanden-Broeck & Tuck 1977; Vanden-Broeck, Schwartz & Tuck 1978; Vanden-Broeck 1985) showed analytically and numerically that there are no continuous solutions for flows past a semi-infinite two-dimensional object with a flat

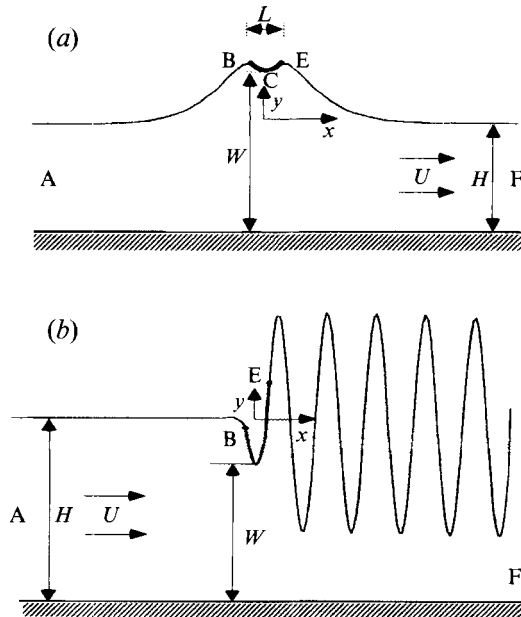


FIGURE 1. Sketch of supercritical flow (a) and subcritical flow (b) past a curved object ( $\epsilon > 0$ ) with continuous tangents at both separation points B and E. The height of the vertex of the object above the bottom is  $W$  and the distance between B and E is  $L$ .

bottom and a vertical front such that the flows approach a uniform stream in the far field and separate at a stagnation point. Dias & Vanden-Broeck (1993) constructed numerically discontinuous solutions by including a model for the breaking of the free surface. On the other hand, Madurasinghe & Tuck (1986) constructed solutions with continuous free-surface profiles for flows past semi-infinite objects by assuming that the free surface attaches tangentially at the separation point. In water of finite depth, there are also continuous solutions for which the flows rise up along the vertical front of the body to a stagnation point at which attachment occurs (see Vanden-Broeck 1989).

All the studies discussed in the previous paragraph are restricted to semi-infinite obstacles. Here we consider objects of finite length. We show numerically that there are continuous supercritical and subcritical solutions for which the free surfaces attach tangentially at the separation points B and E (see figure 1).

An important question is the number of parameters necessary to describe the flows. As we shall see, both supercritical flows and subcritical flows are characterized by three parameters. These parameters are (i) the Froude number  $F$ , (ii) the object geometry  $\epsilon$  (object is concave if  $\epsilon > 0$  and convex if  $\epsilon < 0$ ), (iii) the location of one of the separation points.

For supercritical flows past a concave object ( $F > 1$ ,  $\epsilon > 0$ ), there are two different families of solutions. One family of solutions is characterized by a position of the object below the level of the free surface at infinity. These solutions model a ship moving at a constant velocity in a channel. The other family of solutions is characterized by a position of the object on top of the level of the free surface at infinity. These solutions model an object riding on top of a wave. As  $\epsilon \rightarrow 0$ , they reduce to the 'surfing flows' past a flat plate considered by Vanden-Broeck & Keller (1989).

For supercritical flows past a convex object ( $F > 1$ ,  $\epsilon < 0$ ), there is only one family of solutions for which the position of the object is on top of the level of the free surface

at infinity. These solutions are found to be qualitatively similar to those for flows past a submerged obstruction (see Vanden-Broeck 1987; Dias & Vanden-Broeck 1989; Shen, Shen & Sun 1989). In addition, they are consistent with the analytical findings of Craig & Sternberg (1991).

For subcritical solutions ( $F > 1$ ), the flow is characterized by a train of periodic waves behind the object. We show that these waves become steeper as  $F$  decreases. As  $F$  increases, the amplitude of the waves decreases for a concave object, whereas the amplitude of the waves increases for a convex object.

The supercritical flows are considered in §2. The problem is formulated by using a boundary integral equation technique and the numerical results are presented. The subcritical flows are discussed in §3.

## 2. Supercritical flows ( $F > 1$ )

### 2.1. Formulation

Let us consider the steady two-dimensional irrotational flow of an incompressible inviscid fluid past a parabolic object lying on a free surface in water of finite depth (see figure 1a). We assume that the flow is supercritical and that the object is described by

$$y = \frac{1}{2}\epsilon(x - x_0)^2 + y_0. \quad (2)$$

Here  $(x_0, y_0)$  is the vertex of the object and  $\epsilon$  is a parameter (positive, negative or zero). We choose Cartesian coordinates with the  $x$ -axis along the free surface at infinity and the  $y$ -axis through the vertex of the object. Therefore  $x_0 = 0$ . As  $|x| \rightarrow \infty$ , the flow is required to approach a uniform stream with constant velocity  $U$  and uniform depth  $H$ . The only body force considered here is due to gravity which is acting in the negative  $y$ -direction. We restrict our attention to supercritical solutions which are symmetric with respect to the  $y$ -axis.

We introduce dimensionless variables by choosing  $U$  as the unit velocity and  $H$  as the unit depth. We define the complex potential  $f = \phi + i\psi$  and the complex velocity  $\zeta = df/dz = u - iv$ . Here  $u$  and  $v$  are the components of the velocity in the  $x$ - and  $y$ -directions respectively. Both  $f$  and  $\zeta$  are analytical functions of  $z = x + iy$ . The function  $\zeta$  does not vanish in the flow domain except possibly at the separation points B and E where stagnation points could occur.

Without loss of generality we choose  $\phi = 0$  at the vertex C and  $\psi = 0$  on the free surface AB and EF. By the choice of our dimensionless variables  $\psi = -1$  on the bottom AF.

Consider now the complex function  $u - iv - 1$  which vanishes at infinity. Since the bottom AF is a solid wall, the kinematic boundary condition is satisfied by reflecting the flow domain in the boundary AF. Thus we seek  $u - iv - 1$  as an analytic function of  $f$  in the strip  $-2 \leq \psi \leq 0$ .

To find a relation between  $u(\phi)$  and  $v(\phi)$  on the free surface  $\psi = 0$ , we apply the Cauchy integral formula to the function  $u - iv - 1$  with a contour consisting of the free surface  $\psi = 0$ , the image  $\psi = -2$  of the free surface and two vertical lines at infinity. Thus

$$u(\phi) - iv(\phi) - 1 = -\frac{1}{i\pi} \int_{-\infty}^{\infty} \frac{u(\bar{\phi}) - iv(\bar{\phi}) - 1}{\bar{\phi} - \phi} d\bar{\phi} + \frac{1}{i\pi} \int_{-\infty}^{\infty} \frac{\bar{u}(\bar{\phi}) - i\bar{v}(\bar{\phi}) - 1}{\bar{\phi} - 2i - \phi} d\bar{\phi}. \quad (3)$$

Here  $u, v, \bar{u}$  and  $\bar{v}$  represent the horizontal and vertical velocities on  $\psi = 0$  and  $\psi = -2$  respectively. The first integral in (3) is of Cauchy principal-value form. Using the identities

$$u(\bar{\phi}) = \bar{u}(\phi) \quad \text{and} \quad v(\bar{\phi}) = -\bar{v}(\phi) \quad (4)$$

and the symmetry about  $\phi = 0$

$$u(\bar{\phi}) = u(-\bar{\phi}) \quad \text{and} \quad v(\bar{\phi}) = -v(-\bar{\phi}), \quad (5)$$

we rewrite (3), after taking the real part, as

$$u(\phi) - 1 = \frac{1}{\pi} \int_0^\infty v(\bar{\phi}) \left[ \frac{1}{\bar{\phi} - \phi} + \frac{1}{\bar{\phi} + \phi} \right] d\bar{\phi} \\ + \frac{1}{\pi} \int_0^\infty \frac{2(u(\bar{\phi}) - 1) + v(\bar{\phi})(\bar{\phi} - \phi)}{(\bar{\phi} - \phi)^2 + 4} d\bar{\phi} + \frac{1}{\pi} \int_0^\infty \frac{2(u(\bar{\phi}) - 1) + v(\bar{\phi})(\bar{\phi} + \phi)}{(\bar{\phi} + \phi)^2 + 4} d\bar{\phi}. \quad (6)$$

The atmospheric pressure is assumed to be constant on the free surface. By using the Bernoulli equation we write this condition as

$$\frac{1}{2}q^2 + gy = \frac{1}{2}U^2. \quad (7)$$

Here  $q$  denotes the magnitude of the velocity. In terms of the dimensionless variables, (7) becomes

$$q^2 + \frac{2}{F^2}y = 1, \quad (8)$$

where  $F$  is the Froude number defined in (1).

Using the identity

$$\frac{\partial x}{\partial \phi} + i \frac{\partial y}{\partial \phi} = \frac{1}{\xi}, \quad (9)$$

we can express the kinematic condition on BE as

$$v(\phi) = \epsilon u(\phi) \int_0^\phi \frac{u(\bar{\phi})}{u(\bar{\phi})^2 + v(\bar{\phi})^2} d\bar{\phi}, \quad 0 \leq \phi \leq \phi_e, \quad (10)$$

where  $\epsilon$  is the parameter describing the shape of the parabola in (2) and  $\phi_e$  is the value of the potential function at the separation point E.

On the free surface BA, we can rewrite (8), using (9), in terms of  $u(\phi)$  and  $v(\phi)$ , as

$$u(\phi)^2 + v(\phi)^2 - \frac{2}{F^2} \int_\phi^\infty \frac{v(\bar{\phi})}{u(\bar{\phi})^2 + v(\bar{\phi})^2} d\bar{\phi} = 1, \quad \phi_e < \phi < \infty. \quad (11)$$

For given values of  $\epsilon$ ,  $\phi_e$  and  $F^2$ , (6), (10) and (11) define a system of integro-differential equations for  $u(\phi)$  and  $v(\phi)$ .

Next we introduce the  $M$  mesh points

$$\Phi_i = (i-1)E, \quad i = 1, \dots, M, \quad (12)$$

where  $E$  is the interval of discretization. We shall satisfy (6) and (11) at the midpoints  $\Phi_{i+\frac{1}{2}} = \frac{1}{2}(\Phi_i + \Phi_{i+1})$ ,  $i = 1, \dots, M-1$  and  $\Phi_{i+\frac{1}{2}}$ ,  $i = i_e, \dots, M-1$  respectively. Here  $\Phi_{i_e} = \phi_e$ . The kinematic condition (10) on BE is satisfied at the points  $\Phi_i$ ,  $i = 1, \dots, i_e - 1$ . Thus we obtain  $2M - 2$  nonlinear algebraic equations for the  $2M$  unknowns  $u(\Phi_i)$  and  $v(\Phi_i)$ ,  $i = 1, \dots, M$ . An extra equation is obtained by requiring the velocity at the point E to satisfy both (8) and (10). Eliminating  $v$  between (8) and (10) and solving for  $u$  yields

$$u_e = \left[ \left( 1 - \frac{2}{F^2}y_e \right) / (1 + \epsilon^2 x_e^2) \right]^{\frac{1}{2}}. \quad (13)$$

The last equation is obtained by imposing

$$v(\Phi_M) = 0. \quad (14)$$

The system of  $2M$  nonlinear algebraic equations is solved by Newton's method. Finally, the shape of the free surface is obtained by integrating numerically (9).

## 2.2. Numerical results

We use the numerical scheme described in the previous sub-section to compute solutions for various values of  $F^2$ ,  $\epsilon$  and  $\phi_e$ . We found that the behaviour of the solutions for different values of  $\phi_e > 0$  is qualitatively similar. Thus it is sufficient to present the results for a fixed value of  $\phi_e$ , i.e.  $\phi_e = 0.6$  for various values of  $F^2$  and  $\epsilon$ . The numerical accuracy is checked by increasing  $M$  while keeping  $E$  fixed and vice versa. We find that the results are independent of  $M$  and  $E$ , within graphical accuracy, for  $M \geq 120$  and  $E \leq 0.18$ . All the results presented here were obtained with  $M = 180$  and  $E = 0.1$  and are correct to at least two decimal places unless otherwise mentioned.

As  $\phi_e \rightarrow 0$ , the length  $L$  between the two separation points B and E reduces to zero and we recover the case of a solitary wave. We find that the solitary wave reaches its limiting configuration with a sharp crest and a  $120^\circ$  angle at  $F^2 = 1.69$ . This critical value of the Froude number agrees within 2% with the more accurate value  $F^2 = 1.66$  obtained by Hunter & Vanden-Broeck (1983).

Following Vanden-Broeck & Keller (1989), we define the amplitude parameter

$$\alpha = W/H. \quad (15)$$

Here  $W$  is the distance from the bottom AF to the vertex of the obstacle.

When  $\epsilon = 0$ , the obstacle reduces to a flat plate and we recover the results of Vanden-Broeck & Keller (1989). There is a two-parameter family of flows which bifurcate from the uniform flow, for which  $\alpha = 1$  at  $F^2 = 1$ . As  $\alpha \rightarrow 1$ , the free surfaces tend to approach solutions of the Korteweg-de Vries equation which describes solitary waves of small amplitude:

$$y = (\alpha - 1) \operatorname{sech}^2 \left[ \left( \frac{3}{4(1 + \alpha)} \right)^{\frac{1}{2}} (x \pm \frac{1}{2}L) \right], \quad |x| > \frac{1}{2}L,$$

$$\alpha = F^2.$$

As  $\alpha$  increases, the solutions ultimately reach a limiting configuration with stagnation points and  $120^\circ$  angle corners at B and E. Substituting  $y = \alpha - 1$  and  $q = 0$  into (8), we find that these limiting configurations are characterized by  $\alpha - 1 = \frac{1}{2}F^2$ .

The solutions for  $\epsilon \neq 0$  can be viewed as a perturbation of the solutions for  $\epsilon = 0$ . When  $\epsilon = 0$ , there are two branches of solutions: the uniform flow  $\alpha = 1$  and a branch which bifurcates from the uniform flow at  $F^2 = 1$ . When  $\epsilon \neq 0$ , the uniform flow is no longer a solution for any value of  $F^2$ . Therefore we can expect a perturbed bifurcation from  $F^2 = 1$ .

When  $\epsilon > 0$ , we find two different types of solutions. Solutions of the first type are characterized by  $\alpha - 1 < 0$ , i.e. the vertex of the obstacle is below the level of the free surface at infinity. These solutions model a ship moving at a constant velocity in a channel. A typical profile is shown in figure 2. Solutions of the second type are characterized by  $\alpha - 1 > 0$ , i.e. the vertex of the obstacle is above the level of the free surface at infinity. These solutions model a surfboard riding on a wave. A typical profile of a solution of this type is shown in figure 5. The numerical values of  $F^2$  versus  $\alpha - 1$  for a fixed value of  $\phi_e$ , and various values of  $\epsilon$  are shown in figure 3.

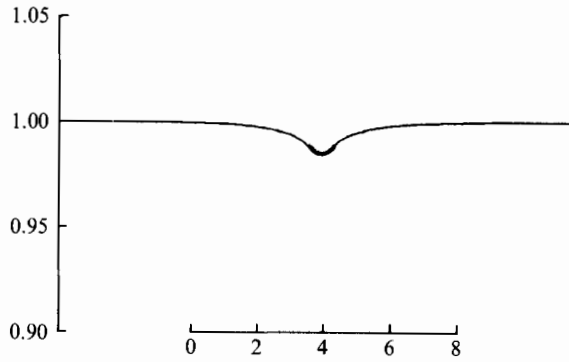


FIGURE 2. Computed free-surface profile of the flow corresponding to solutions of the first type,  $\alpha - 1 < 0$ , for  $F^2 = 1.55$ ,  $\epsilon = 0.05$  and  $\phi_e = 0.6$ .

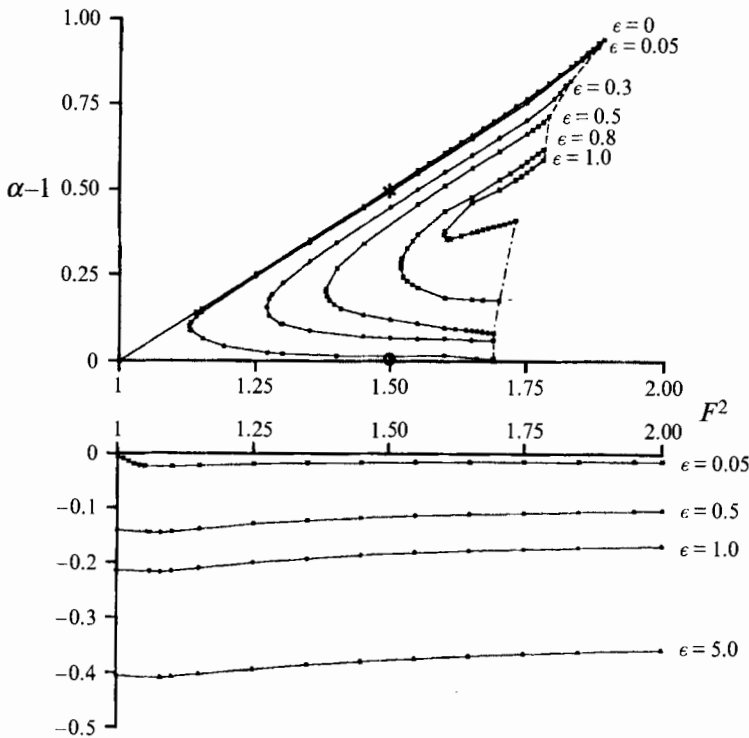


FIGURE 3. Values of the dimensionless height  $(W - H)/H = \alpha - 1$  of the vertex of the object above the free-surface level at infinity versus  $F^2$  for various values of  $\epsilon$  and  $\phi_e = 0.6$ . The dashed curve at the top of the figure corresponds to the limiting cases in which stagnation points with  $120^\circ$  angle occur at the edges of the object. The dot-dash curve corresponds to the limiting cases in which the crests of the bumps reach their maximum heights.

The solutions of the first type,  $\alpha - 1 < 0$ , can be viewed as perturbations of a uniform flow (i.e. they approach the uniform stream as  $\epsilon \rightarrow 0$  for a fixed value of  $F^2$ ). These branches of solutions extend from  $F^2 = 1$  to  $F^2 = \infty$  (see figure 3). We expect that these branches can be extended to the subcritical regime ( $F^2 < 1$ ) by allowing waves downstream. Solutions with waves will be considered in the next section.

The solutions of the second type,  $\alpha - 1 > 0$ , can be viewed as perturbations of the branch of solutions with  $\epsilon = 0$  which bifurcate from  $F^2 = 1$ . On these branches of

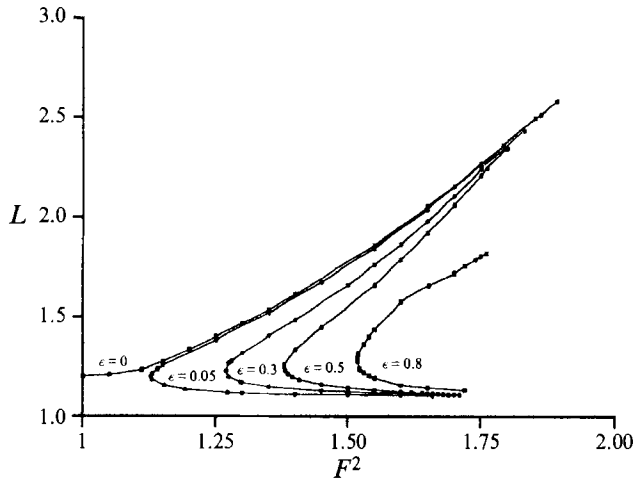


FIGURE 4. Values of  $L$  versus  $F^2$  for solutions of the second type,  $\alpha - 1 > 0$  with  $\phi_e = 0.6$ .

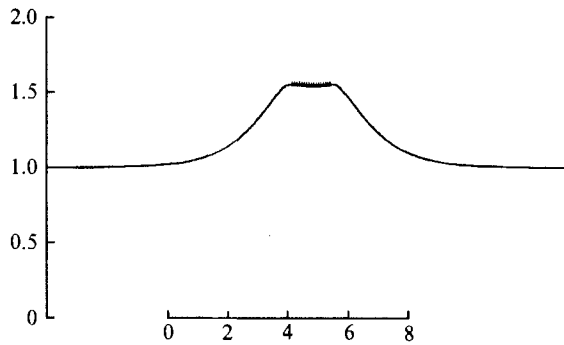


FIGURE 5. Computed free-surface profile of the flow corresponding to solutions of the second type,  $\alpha - 1 > 0$ , for  $F^2 = 1.5$ ,  $\epsilon = 0.05$  and  $\phi_e = 0.6$ . This solution corresponds to (\*) in figure 3.

solutions, there are three critical values,  $\tilde{F}_1^2$ ,  $\tilde{F}_2^2$  and  $\tilde{F}_3^2$ , of  $F^2$  such that, for each  $\epsilon$ , there are no solutions for  $F^2 < \tilde{F}_2^2$  and  $F^2 > \tilde{F}_1^2$ , two solutions for  $\tilde{F}_2^2 < F^2 < \tilde{F}_3^2$ , and one solution for  $\tilde{F}_3^2 < F^2 < \tilde{F}_1^2$ . They can easily be seen in figure 3: the critical values  $\tilde{F}_2^2$  are the turning points, the critical values  $\tilde{F}_3^2$  are on the lower dot-dash curve and the critical values  $\tilde{F}_1^2$  are on the upper dashed curve. Stagnation points with corners occur at the separation points B and E when  $F^2 = \tilde{F}_1^2$ . The angle of the corners depends on the local slope  $\delta$  of the obstacle at the separation points (Dagan & Tulin 1972). If  $\delta$  at E is smaller than  $\sqrt{3}$ , then the angle of the corner is  $120^\circ$ . If  $\delta > \sqrt{3}$ , then the angle of the corner is  $90^\circ$ . In all our computation,  $\delta$  was always smaller than  $\sqrt{3}$ . It can be shown, by substituting  $y = \alpha - 1$  and  $q = 0$  into (8) and using (2), that these limiting configurations are characterized by

$$\alpha - 1 = \frac{1}{2}(F^2 - \frac{1}{4}L^2\epsilon). \tag{16}$$

The limiting configurations cannot be calculated directly by our scheme since we assumed that the flow leaves the obstacle tangentially. However we were able to compute solutions very close to the limiting configurations. Values of  $L$  versus  $F^2$  are presented in figure 4. Relation (16) corresponds to the upper dashed curve in figure 3. A typical profile for a value of  $\tilde{F}_2^2 < F^2 < \tilde{F}_1^2$  is shown in figure 5.

Near  $F^2 = \tilde{F}_2^2$ , 'bumps' (or 'valleys') appear on the free surfaces. These bumps are

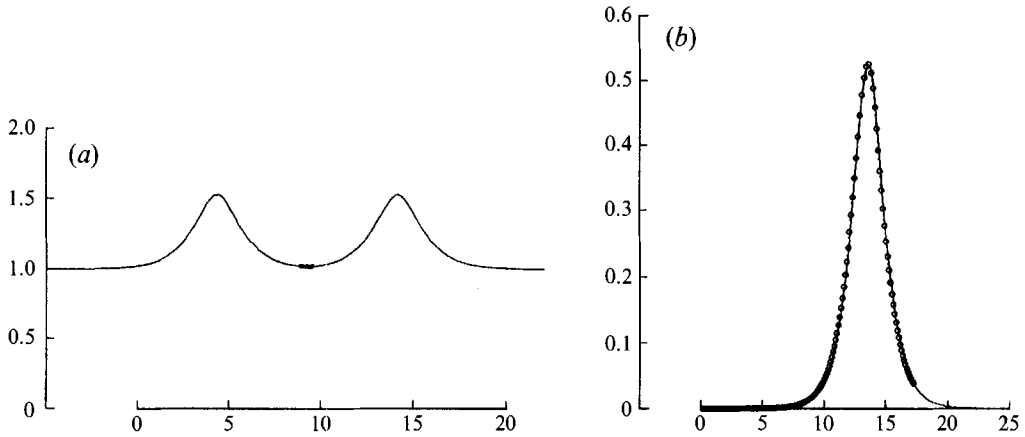


FIGURE 6. (a) Computed profile of flow for  $F^2 = 1.5$ ,  $\epsilon = 0.05$  and  $\phi_e = 0.6$ . This solution corresponds to (o) in figure 3. (b) Comparison between the crests of the bumps (o) in (a) with the solitary wave (—) corresponding to  $F^2 = 1.5$ .

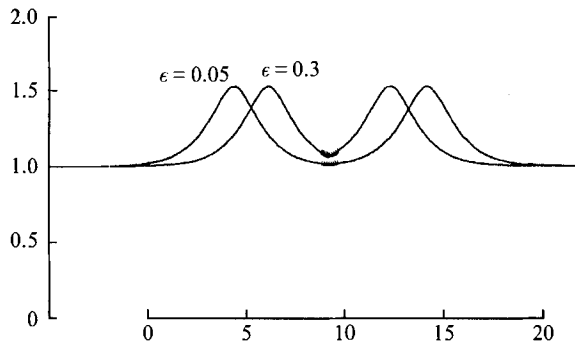


FIGURE 7. Two supercritical profiles for  $\epsilon = 0.05$  and  $0.3$  corresponding to the same values of  $F^2 = 1.5$  and  $\phi_e = 0.6$ .

not far away from the obstacle when  $F^2$  is close to  $\tilde{F}_2^2$ . However, as  $F^2$  increases along the lower portion of the curve for a fixed  $\epsilon$  in figure 3, the distance between the crests of the bumps and the separation points increases. Furthermore, the elevation of the crests of these bumps above the level of the free surface at infinity also increases. Typical profiles of such flows are shown in figures 6 and 7. When the bumps occur far from the obstacle, their shape tends to approach a solitary wave. This is illustrated in figure 6(b) where we compare the bump for  $F^2 = 1.5$ ,  $\epsilon = 0.05$  and  $\phi_e = 0.6$  with the solitary wave corresponding to the same Froude number.

The height of the bumps increases progressively as  $F^2$  increases and ultimately the bumps reach limiting configurations with stagnation points and  $120^\circ$  angles at their crests when  $F^2 = \tilde{F}_3^2$  (lower dot-dash curve in figure 3). Figure 7 shows a comparison of profiles with bumps at the same value of  $F^2$  for different values of  $\epsilon$ . The heights of the bumps are approximately at the same level. However, the bumps move farther away from the separation points as  $\epsilon$  decreases. We expect that the solutions will approach the uniform flow as  $\epsilon$  reduces to zero for a fixed  $F^2$ . The approach is non-uniform in the sense that the amplitude of the bumps does not decrease: they simply move to infinity as  $\epsilon \rightarrow 0$ .

For the case  $\epsilon < 0$ , the solutions are found to be, qualitatively, similar to those for the flows past a submerged obstruction (Forbes & Schwartz 1982; Vanden-Broeck

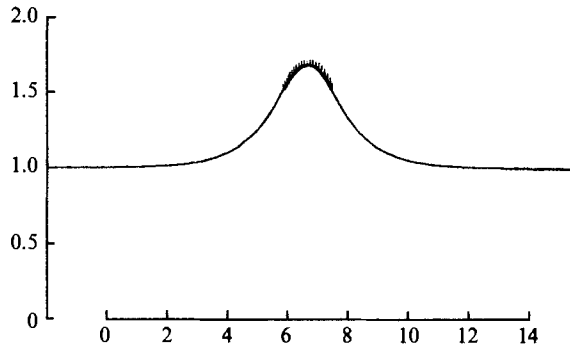


FIGURE 8. Computed profile of flow for  $F^2 = 1.65$ ,  $\epsilon = -0.5$  and  $\phi_b = 0.6$ .

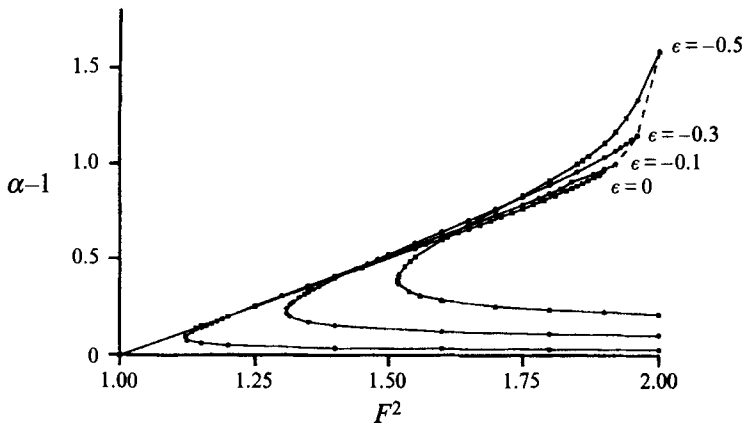


FIGURE 9. Values of  $\alpha - 1$  versus  $F^2$  for  $\phi_e = 0.6$  and four values of  $\epsilon < 0$ . The dashed curve corresponds to the limiting cases for which stagnation points with a  $120^\circ$  angle occur at the edges of the object.

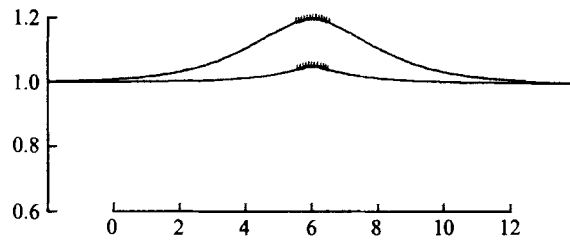


FIGURE 10. Two supercritical profiles corresponding to the same values of  $F^2 = 1.2$ ,  $\epsilon = -0.1$  and  $\phi_e = 0.6$ . The solution with the higher elevation corresponds to a perturbation of the solution with  $\epsilon = 0$  of Vanden-Broeck & Keller (1989). The solution with the lower elevation corresponds to a perturbation of a uniform stream.

1987; Dias & Vanden-Broeck 1989; Shen *et al.* 1989). A typical profile is shown in figure 8. Numerical values of  $\alpha - 1$  versus  $F^2$  for various values of  $\epsilon$  and  $\phi_e = 0.6$  are presented in figure 9. A comparison of figures 3 and 9 shows that the solutions for  $\epsilon < 0$  do not have the same behaviour as the solutions for  $\epsilon > 0$ . Here there are only two critical values  $1 < \tilde{F}_4^2 < \tilde{F}_5^2$  of  $F^2$ , for each  $\epsilon$  and  $\phi_e$ , such that there are no solutions for  $F^2 < \tilde{F}_4^2$ , two solutions for  $\tilde{F}_4^2 < F^2 < \tilde{F}_5^2$ , and a unique solution for  $F^2 > \tilde{F}_5^2$ . It can be seen from figure 9 that, as  $\alpha - 1$  increases,  $F^2$  first decreases to a minimum value  $\tilde{F}_4^2$  and

then increases up to a critical value  $\tilde{F}_5^2$ . The values  $\tilde{F}_5^2$  are on the dashed curve which agrees with relation (16). Solutions for  $F^2 = \tilde{F}_5^2$  corresponds to profiles with stagnation points at both separation points with an angle of  $120^\circ$ . The lower portion of the solid curves in figure 9 corresponds to solutions that are perturbation of the uniform stream, whereas the upper portion of the curves corresponds to solutions that are perturbations of the solutions of Vanden-Broeck & Keller (1989) for  $\epsilon = 0$ . These two types of solutions are shown in figure 10.

### 3. Subcritical flows ( $F < 1$ )

We use the boundary integral equation technique developed in §2 to calculate subcritical flows past a surface-piercing obstacle. Unlike supercritical solutions, subcritical solutions have a train of waves behind the obstacle and a net horizontal drag force exerted on the wetted surface of the obstacle (see figure 1*b*).

The flow upstream is uniform with velocity  $U$  and depth  $H$ . We select  $U$  as the reference velocity and  $H$  as the reference depth. A slight change in the choice of the coordinate axis is made here because the abscissa of the vertex of the obstacle is not known in advance. We choose the  $x$ -axis along the free surface at  $x = -\infty$  and the  $y$ -axis through the separation point B at which  $\phi = 0$  (see figure 11). By the choice of our dimensionless variables, the Froude number  $F$  is defined as in (1). The shape of the obstacle is described by (2).

Proceeding as in §2.1, we obtain the same integral equation (3). Since there is no symmetry with respect to the  $y$ -axis for the subcritical case, the domain of integration in (3) cannot be reduced to the one in (6). Using (4) and taking the real part of (3), we obtain the integral equation for the velocity components on the free surface:

$$u(\phi) - 1 = \frac{1}{\pi} \int_{-\infty}^{\infty} \frac{v(\bar{\phi})}{\bar{\phi} - \phi} d\bar{\phi} + \frac{1}{\pi} \int_{-\infty}^{\infty} \frac{v(\bar{\phi})(\bar{\phi} - \phi) + 2(u(\bar{\phi}) - 1)}{(\bar{\phi} - \phi)^2 + 4} d\bar{\phi} \quad \text{on } \psi = 0. \quad (17)$$

The kinematic condition on BE is

$$v(\phi) = \epsilon u(\phi)(x - x_0). \quad (18)$$

It is convenient to eliminate the term  $(x - x_0)$  in (18) by differentiating (18) with respect to  $\phi$ . Using the fact that  $\partial x / \partial \phi = u / (u^2 + v^2)$  and the relation (18) itself, we obtain the new expression for the kinematic condition on BE:

$$v_\phi(\phi) = u_\phi(\phi) \frac{v(\phi)}{u(\phi)} + \frac{\epsilon u^2(\phi)}{u^2(\phi) + v^2(\phi)} \quad \text{on BE}. \quad (19)$$

The free-surface boundary condition remains as it was in (8). The radiation condition prohibiting the upstream disturbances must also be satisfied, i.e.

$$u \rightarrow 1, v \rightarrow 0 \quad \text{as } \phi \rightarrow -\infty. \quad (20)$$

We impose (13) at the separation point B to ensure that the free surface makes contact with the obstacle with a continuous tangent. For a given value of  $F$ ,  $\epsilon$  and  $\phi_e$ , the system of equations (17), (19), (20) and (8) determines the velocity components  $(u(\phi), v(\phi))$  on the free surfaces and the obstacle. Once  $u$  and  $v$  are known, we can calculate the profile of the free surfaces by integrating (9) over the streamline  $\psi = 0$ .

The wave drag  $D$  is calculated by integrating the pressure  $p$  over the obstacle wetted surface. That is

$$D = \int_{\text{obstacle surface}} p n_x ds = -\frac{\epsilon}{2} \int_0^L \left( 1 - q^2 - \frac{2y}{F^2} \right) (x - x_0) dx. \quad (21)$$

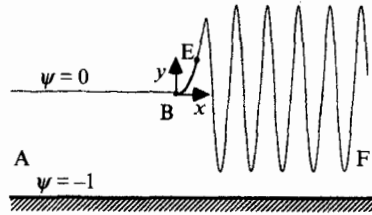


FIGURE 11. Sketch of a subcritical flow with a change in the choice of the coordinate axis.

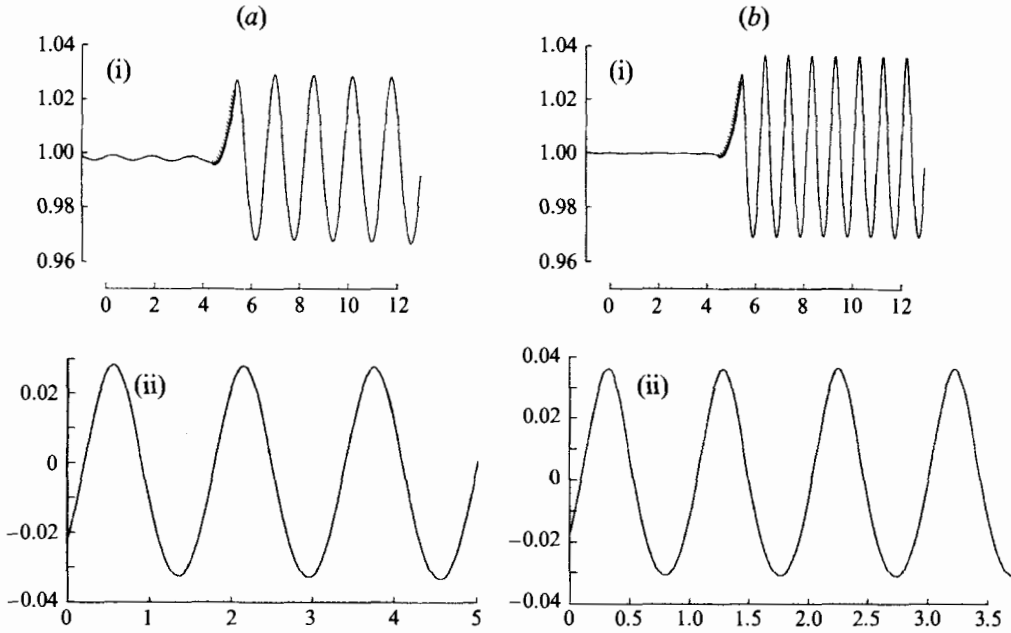


FIGURE 12. (i) Computed profile for  $\epsilon = 0.075$  and  $\phi_e = 0.91$ : (a)  $F = 0.5$ , (b)  $F = 0.4$ . (ii) Blow up of the downstream train of waves in (i). In (a) the waves are close to linear sine waves, while in (b) they are clearly nonlinear with broad troughs and sharp crests.

Here  $n_x$  is the  $x$ -component of the outward unit normal vector to the obstacle. The wave drag is made dimensionless by reference to the quantity  $\rho g H^2$ , where  $\rho$  is the density of the fluid. After being transformed into the  $f$ -plane, (21) becomes

$$D = -\frac{1}{2} \int_0^{\phi_e} \left( 1 - q^2 - \frac{2y}{F^2} \right) \frac{v}{u^2 + v^2} d\phi. \quad (22)$$

The numerical procedure follows closely the procedure described in §2. The derivatives  $u_\phi$  and  $v_\phi$  in (19) are approximated by

$$\left. \begin{aligned} (u_\phi)_{i-\frac{1}{2}} &= \frac{u_{i+1} - u_i}{E} \\ (v_\phi)_{i-\frac{1}{2}} &= \frac{v_{i+1} - v_i}{E} \end{aligned} \right\}, \quad i = i_b, \dots, i_e - 1. \quad (23)$$

where  $E$  is the interval of discretization. Here  $u_{i_b} = u(\phi = 0)$ ,  $v_{i_b} = v(\phi = 0)$ ,  $u_{i_e} = u(\phi = \phi_e)$  and  $v_{i_e} = v(\phi = \phi_e)$  denote the velocity components at the separation points.

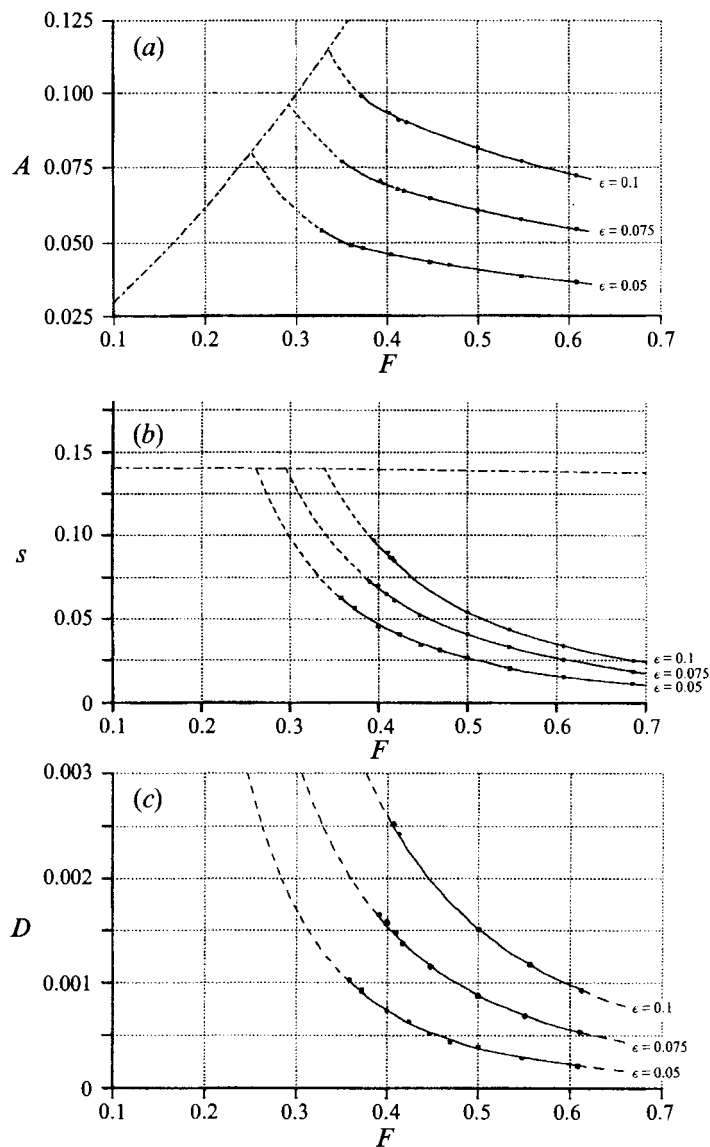


FIGURE 13. (a) The amplitude  $A$  of the waves versus  $F$ ; (b) the steepness  $s$  of the waves versus  $F$ ; (c) the dimensionless wave drag  $D$  versus  $F$ . The dot-dash curve in (a) and (b) corresponds to the limiting cases characterized by a  $120^\circ$  angle at the crests (Cokelet 1977). The dashed curves are the extrapolated results.

The numerical results show that subcritical solutions depend on three parameters,  $F$ ,  $\epsilon$  and  $\phi_e$ . It is observed that the behaviour of the solutions is qualitatively similar for different values of  $\phi_e$ . Thus, it is sufficient to present results at one particular value:  $\phi_e = 0.91$ . The solution reduces to a uniform flow when  $\epsilon = 0$ .

Typical profiles for  $\epsilon > 0$  are shown in figure 12. These nonlinear solutions are obtained with  $N = 600$  and  $E = 0.035$ . At a distance of about one wavelength aft of the obstacle, the wavetrain is essentially periodic. Figure 13(a) shows that the amplitude  $A$  of the waves, defined as the difference between the levels of a successive crest and trough, increases as  $F$  decreases. In addition, the steepness  $s$  of the waves,

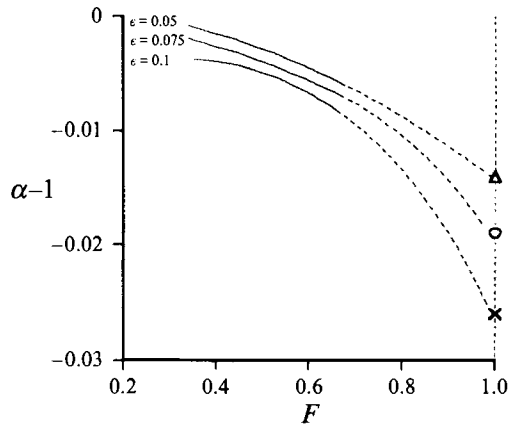


FIGURE 14. Values of  $(W-H)/H = \alpha - 1$  versus  $F$  for some values of  $\epsilon > 0$ . The dashed curves are the extrapolated results. The values of  $\alpha - 1$  at  $F = 1$ , ( $\Delta$ ,  $\circ$  and  $\times$ ) are obtained by using the scheme in §2.

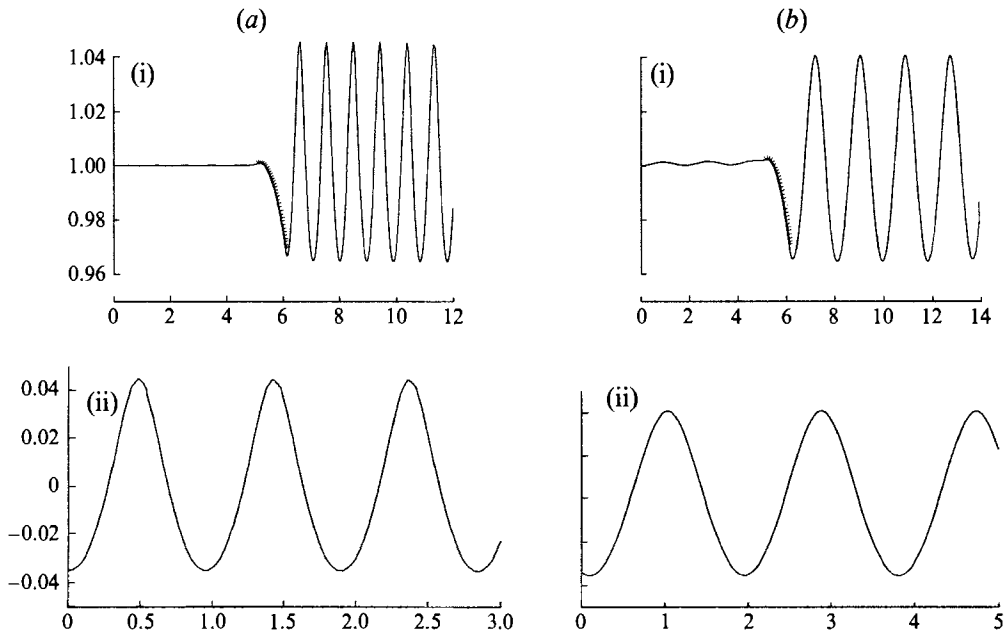


FIGURE 15. (i) Computed profile for  $\epsilon = -0.075$  and  $\phi_e = 0.91$ : (a)  $F = 0.4$ , (b)  $F = 0.55$ . (ii) Blow up of the downstream train of waves in (i). In (a) the waves are clearly nonlinear with broad troughs and sharp crests, while in (b) they are close to linear sine waves.

defined as the difference of heights between a crest and a trough divided by the wavelength, is shown to be a decreasing function of  $F$  in figure 13(b). For large values of  $F$ , the waves appear to be close to linear sine waves (see figure 12a). These waves tend to develop narrow crests and broad troughs showing the nonlinearity of the waves as  $F$  decreases (see figure 12b). As  $F$  decreases to the critical value  $F^*$ , the elevation of the crests tends to the stagnation level  $\frac{1}{2}(F^*)^2$  and the waves reach their limiting configuration characterized by a  $120^\circ$  angle at the crests. In order to obtain these critical values, it is necessary to have a finer mesh to resolve the sharp crests. This

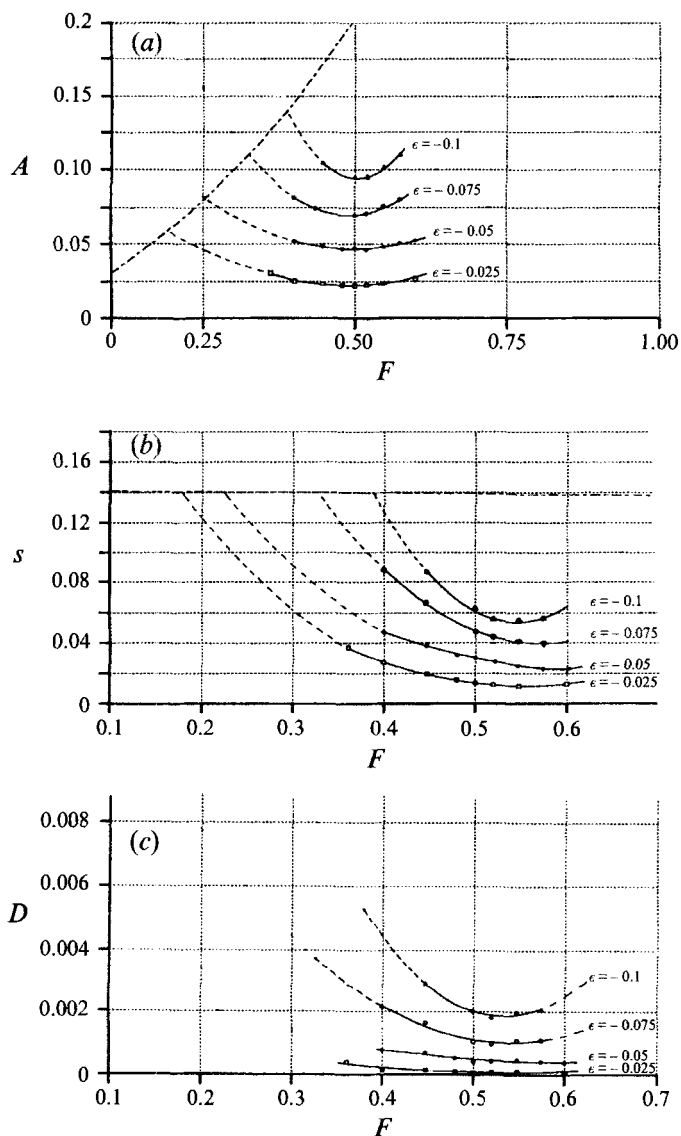


FIGURE 16. (a) The amplitude  $A$  of the waves versus  $F$ ; (b) the steepness  $s$  of the waves versus  $F$ ; (c) the dimensionless wave drag  $D$  versus  $F$ . The dot-dash curve in (a) and (b) corresponds to the limiting cases characterized by a  $120^\circ$  angle at the crests (Cokelet 1977). The dashed curves are the extrapolated results.

requires an extensive use of computer time. The dashed curves in figures 13(a) and 13(b) are the extrapolations of the computed solutions (solid curves). Here and in the remaining part of the paper, all the extrapolations are obtained by fitting a second-order polynomial curve by a linear least-squares regression technique. The dot-dash curves in both figures correspond to the highest waves computed by Cokelet (1977).

Figure 13(c) shows the computed values of the wave drag  $D$  versus  $F$ . The numerical values of  $\alpha - 1$ , defined in (15), versus  $F$  are also presented in figure 14. Difficulties arise in the numerical computation as we attempt to calculate solutions for values of  $F$  close to one. This is because the waves become very long. The converged solutions incorrectly predict small periodic disturbances on the upstream free surface (see figure

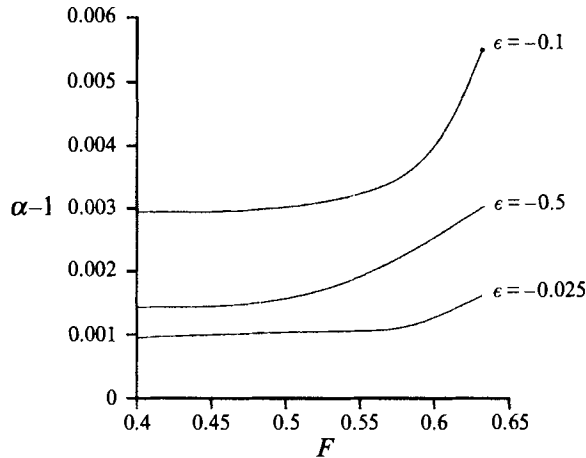


FIGURE 17. Values of  $\alpha - 1$  versus  $F$  for some values of  $\epsilon < 0$ .

12a). This indicates that farther truncation downstream of the integral in (17) and more mesh points are needed. We are able to obtain solutions up to  $F = 0.7$ . As we can see, the wave steepness  $s$ , the wave amplitude  $A$ , and the wave drag  $D$  decrease progressively as  $F$  increases. It is possible that the supercritical solutions (branch of solutions with  $\alpha - 1 < 0$ ) are the continuations of the present branch of solutions. This is suggested by figure 14. In this figure we extrapolate the computed solutions (solid curves) and show also the values  $\alpha - 1$  at  $F = 1$  obtained by using the numerical scheme developed in §2. The extrapolated results (dotted curves) show a good agreement at  $F = 1$ .

Typical profiles for  $\epsilon < 0$  are shown in figures 15(a) and 15(b). We observe that the behaviour of the solutions is similar to those for  $\epsilon > 0$  in the low-speed region (small  $F$ ), that is the nonlinear effects are apparent when  $F$  is small. As  $F$  decreases, the wave aft of the obstacle begins to develop sharp crests and broad troughs (see figure 15a), and ultimately break when the crests become stagnation points with a  $120^\circ$  angle as  $F \rightarrow F^{**}$ . However, the waves appear to be close to linear sine waves when  $F$  increases as shown in figure 15(b). In figure 16(a-c), we show that the wave amplitude  $A$ , the wave steepness  $s$ , and the wave drag  $D$  decrease to minimum values  $A_{min}$ ,  $s_{min}$ , and  $D_{min}$ , and then increase as  $F$  increases.

The numerical values of  $\alpha - 1$  versus  $F$  are presented in figure 17. In §2, we found that, for  $\epsilon < 0$ , there are no supercritical solutions when  $F \downarrow 1$ . This is clearly shown in figure 9 where the plots of  $\alpha - 1$  versus  $F^2$  have turning points for  $F > 1$ . Therefore the subcritical solutions for  $\epsilon < 0$  cannot be continuously continued by the supercritical solutions as we expect in the case  $\epsilon > 0$  (see the lower curves in figure 3 which extend to  $F^2 = 1$ ). Since  $A$ ,  $s$  and  $D$  ultimately increase as  $F$  increases, we expect the waves to break when  $F$  reaches a critical value  $F^{***}$ . Such a behaviour was observed by Forbes & Schwartz (1982) for the flow past a submerged obstruction on the bottom of a channel.

In addition to the occurrence of small periodic disturbances on the upstream free surface when  $F$  is large, we found that the nonlinear profile begin to deviate from a periodic wave train. It is observed that the upstream disturbances grow as the amplitude of the waves increases. Owing to these numerical difficulties, we only present solutions for  $F < 0.6$ .

Finally let us mention that the numerical procedures described in this paper can

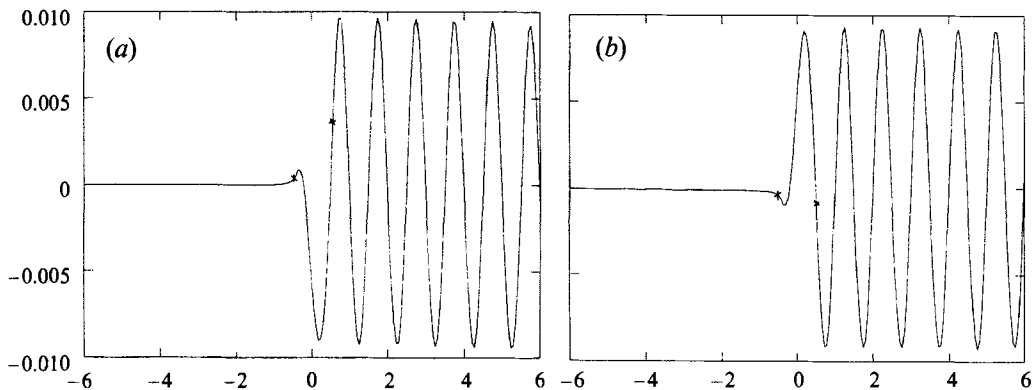


FIGURE 18. Free-surface profile for the distribution of pressure defined by (24) and (25) with  $F = 0.4$ ,  $b = 0.5$ . The two crosses correspond to  $x = -b$  and  $x = b$ . (a)  $\delta = 0.1$ , (b)  $\delta = -0.1$ .

easily be adapted to study the flow past a prescribed distribution of pressure. As an example we present in figures 18(a) and 18(b) and, free-surface flows past the distribution of pressure defined by

$$p(x) = 0, \quad |x| > b \quad (24)$$

and

$$p(x) = \delta \exp\left[\frac{b^2}{x^2 - b^2}\right], \quad |x| < b \quad (25)$$

for  $F = 0.4$  and  $b = 0.5$ . In figure 18(a),  $\delta = 0.1$  and the pressure is positive for  $|x| < b$ . In figure 18(b),  $\delta = -0.1$  and the pressure is negative for  $|x| < b$ . Such solutions also describe the flow past an obstacle if the portion of the free surface for  $|x| < b$  is replaced by a rigid surface.

This work was supported by the National Science Foundation.

#### REFERENCES

- COKELET, E. D. 1977 *Phil. Trans. R. Soc. Lond. A* **286**, 183.  
 CRAIG, W. & STERNBERG, P. 1991 *J. Fluid Mech.* **230**, 231.  
 DAGAN, G. & TULIN, M. P. 1972 *J. Fluid Mech.* **51**, 529.  
 DIAS, F. & VANDEN-BROECK, J.-M. 1989 *J. Fluid Mech.* **206**, 155.  
 DIAS, F. & VANDEN-BROECK, J.-M. 1993 *J. Fluid Mech.* **255**, 91.  
 FORBES, L. K. & SCHWARTZ, L. W. 1982 *J. Fluid Mech.* **114**, 299.  
 HUNTER, J. K. & VANDEN-BROECK, J.-M. 1983 *J. Fluid Mech.* **136**, 63.  
 MADURASINGHE, M. A. D. & TUCK, E. O. 1986 *J. Austral. Math. Soc. B* **27**, 442.  
 SHEN, S. P., SHEN, M. C. & SUN, S. M. 1989 *J. Engng Maths* **23**, 315.  
 VANDEN-BROECK, J.-M. 1980 *J. Fluid Mech.* **96**, 603.  
 VANDEN-BROECK, J.-M. 1985 *Advances in Nonlinear Waves*, Vol. II (ed. L. Debnath). Pitmann, Boston.  
 VANDEN-BROECK, J.-M. 1987 *Phys. Fluids* **30**, 2315.  
 VANDEN-BROECK, J.-M. 1989 *Phys. Fluids A* **1**, 1328.  
 VANDEN-BROECK, J.-M. & KELLER, J. B. 1989 *J. Fluid Mech.* **198**, 115.  
 VANDEN-BROECK, J.-M., SCHWARTZ, L. W. & TUCK, E. O. 1978 *Proc. R. Soc. Lond. A* **361**, 207.  
 VANDEN-BROECK, J.-M. & TUCK, E. O. 1977 *Proc. 2nd Intl Conf. on Numerical Ship Hydrodynamics, Berkeley, CA*, p. 371.